Extreme ultraviolet holographic microscopy and its application to extreme ultraviolet mask-blank defect characterization

Sang Hun Lee[a)] and Jeffrey Bokor
Department of Electrical Engineering and Computer Science, University of California, Berkeley, Claifornia 94720 and Center for X-Ray Optics, Lawrence Berkeley National Laboratory, Berkeley, California 94720

Patrick Naulleau, Seong Tae Jeong, and Kenneth A. Goldberg
Center for X-Ray Optics, Lawrence Berkeley National Laboratory, Berkeley, California 94720

(Received 1 June 2000; accepted 22 July 2000)

100-nm-resolution at-wavelength holographic microscopy of aerial images produced by extreme ultraviolet (EUV) lithographic optics has recently been demonstrated. It provides a simple and compact method allowing image monitoring without printing in photoresist. Here, the concept of holographic microscopy is extended to the characterizations of defects on EUV multilayer mask blanks. As a proof of principle, defect characterization using the holographic microscope is demonstrated with programmed defects in transmission masks. Amplitude defects as small as 100 nm have been successfully characterized. Extension of this technique to the more relevant reflection mask configuration is also discussed. © *2000 American Vacuum Society.*
[S0734-211X(00)02506-3]

I. INTRODUCTION

EUV lithography optics require unprecedented fabrication tolerances[1] and hence unprecedented metrology accuracy. We have recently demonstrated an at-wavelength holographic microscopy technique developed to monitor the coherent imaging performance of high quality extreme ultraviolet (EUV) lithographic optical systems at 13.4 nm wavelength.[2,3] This technique provides a simple and compact method for recording aerial images without printing in photoresist. Even though the holographic method is restricted to coherent imaging, while lithographic printing typically employs partially coherent light, the partially coherent imaging performance can be readily predicted from the coherent image. 100-nm-resolution holographic reconstructions of various image distributions, including ones due to phase-shift-enhanced masks, have been experimentally demonstrated and verified by way of computer simulation.[2,3]

Here we present the extension of the holographic microscopy concept to the characterization of defects on EUV multilayer mask blanks. A significant concern for the commercial viability of EUV lithography is defect control on the requisite reflective multilayer masks.[4] Because there are no known methods to correct defects in and on a multilayer, it is crucial to identify the defects providing feedback for the development of a nearly zero-defect multilayer mask fabrication process. Tremendous progress toward the zero-defect goal has been achieved using conventional wafer inspection methods as the feedback mechanism.[4] Obtaining adequate sensitivity to both phase and amplitude defects at the relevant sizes, however, is an extremely challenging task for these conventional tools. At-wavelength characterization, providing a more direct probe of the EUV optical properties of defects, is thus crucial to the optimization of conventional metrology tools.

To address the at-wavelength mask-bank inspection concerns, an EUV scanner based on raster scanning a focused EUV spot along the EUV mask blank has recently been developed.[5] This system has the capability of identifying the locations of both amplitude and phase defects on multilayer mask blanks. To enhance this system's capability to characterize defects, it would be desirable to add a holographic microscope to the scanner. In this combined device, the defects would be located using the EUV scanner and then characterized using the built-in holographic microscope. The holographic method is of particular interest because few other methods can quantify both the phase and amplitude of submicron sized defects on EUV mask blanks.

In this work, we validate the concept of using the holographic microscope as an EUV mask-blank defect inspection tool by characterizing programmed defects on simple transmission masks. In this demonstration, we consider amplitude defect sizes ranging from 500 to 70 nm. Extension of this technique to the more relevant reflection mask configuration is also discussed.

II. EXPERIMENTAL SETUP

The schematic diagram of the proof-of-principle transmission configuration is shown in Fig. 1. The system is based on the principles of lensless Fourier-transform holography[6] and has been implemented by modifying the EUV phase-shifting point diffraction interferometer (PS/PDI) developed at Lawrence Berkeley National Laboratory.[7]

a)Electronic mail: shlee@eecs.berkeley.edu

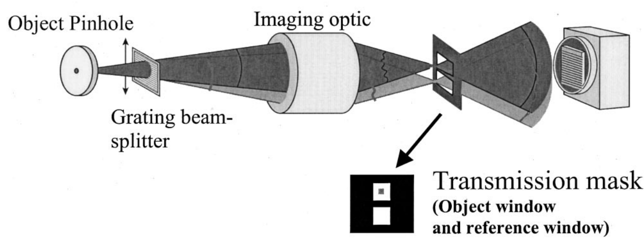

FIG. 1. Schematic of a holographic microscopy system to characterize a program defect in a transmission mask. The system is obtained by slight modification of the PS/PDI system. The imaging optic is illuminated with uniform coherent light.

A spatial filtering pinhole is used to produce a spatially coherent spherical wave front that illuminates the imaging optic. The pinhole size is chosen to yield relatively uniform illumination within the entrance pupil of the optic. A transmission grating is inserted between the object pinhole and the optical system to act as a beam splitter, producing multiple, laterally displaced, focal points in the image plane of the optical system. A transmission mask containing two windows is placed near the image plane to select two of the orders diffracted by the grating. The rest of the mask is made opaque in order to block all remaining grating-order terms avoiding confusion in the data analysis. One of the windows contains the programmed defect whereas the other window has no defect (Fig. 2). From the point of view of holography, the beam passing through the window with the defect serves as the object beam while the beam passing through the clean window serves as the reference. The two beams propagate to the charge-coupled device (CCD) camera where they overlap producing a hologram. The hologram captures a record of the complex-valued diffraction pattern created by the defect and can be used to reconstruct an image of the defect itself.

The imaging optic used in this experiment is a Schwarzschild objective with 10× demagnification. The optic is comprised of two spherical Mo/Si multilayer-coated mirrors, has numerical aperture (NA) of 0.088, and 400-μm-diam image-side field of view. The wave front quality of the optic has been measured with the PS/PDI to be approximately $\lambda/20$ root-mean-square (rms) over 0.088 NA at a wavelength of 13.4 nm.[7]

The image-side transmission mask containing the two windows is placed about 12 μm beyond the image plane. The mask is intentionally placed out of focus allowing a larger window area to be observed. In this way, large or multiple defects may be characterized in parallel, minimizing

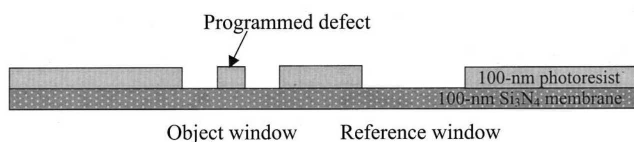

FIG. 2. Diagram of the transmission mask cross section. The photoresist was used for necessary EUV attenuation on top of nitride membrane. The object window contains square defects sized from 500 to 70 nm, and the defects are amplitude defects and also made with the photoresist.

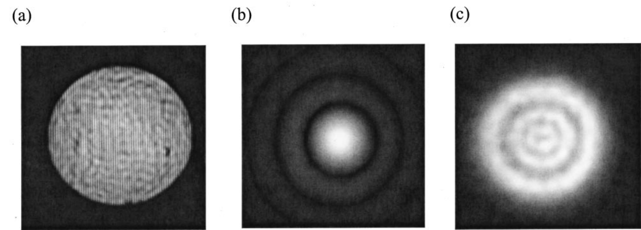

FIG. 3. Typical hologram recorded with no defect in the transmission mask. (b) Fourier transform. The Fourier transform represents the reconstruction of the image plane distribution. The almost perfect reconstructed Airy pattern is a result of the errors in the reference and object waves canceling each other out. (c) Defect-free intensity reconstruction after Fresnel propagation to the mask plane.

the need for scanning the probe beam across the area of interest. The beam size at the mask plane is about 2 μm in diameter. This size is chosen to be larger than any defect size of interest yet smaller than the size of the window itself.

The two windows have dimensions of 2.5 μm×2.5 μm each with a center-to-center separation of 5 μm. The center-to-center separation is 2 times the window width preventing overlap between the holographic image and the zero order image.[3] The object window contains programmed square amplitude defects with sizes ranging from 500 to 70 nm. A diagram of the transmission mask cross section is shown in Fig. 2. The mask is fabricated onto 1000 Å Si_3N_4 membranes using electron beam lithography. The EUV attenuation for opaque areas of the mask and the programmed amplitude defects is provided by a 1000-Å-thick film of photoresist. Use of photoresist as the attenuation medium facilitated the mask fabrication process.

The object beam, which carries information about the defect, and the reference beam, which is simply a diverging spherical beam, interfere to generate hologram on a CCD detector placed approximately 100 mm from the image plane. The detector is a back-illuminated, back-thinned, EUV CCD detector with 1024 by 1024 pixels over 1-sq-in. area. The required exposure time is usually less than 1 s.

III. EXPERIMENTAL RESULTS

The method used to reconstruct the programmed defects from the recorded holograms is described as follows. Because the defect is placed out of the focal plane, the recorded hologram is not, strictly speaking, a Fourier-transform hologram. Simple Fourier-transform processing would reconstruct the field in the focal plane, whereas we are interested in the field in the defect plane. From the field in the focal plane, however, we can readily calculate the field in the defect plane by Fresnel propagation. The time required to analyze the data is relatively short when the location of the mask plane is well known. In practice, we have found the data analysis to take approximately 30 s, although no effort has been made to optimize the process.

A typical hologram recorded with no defect in the transmission mask is shown in Fig. 3(a), along with its Fourier transform, Fig. 3(b). The Fourier transform represents the

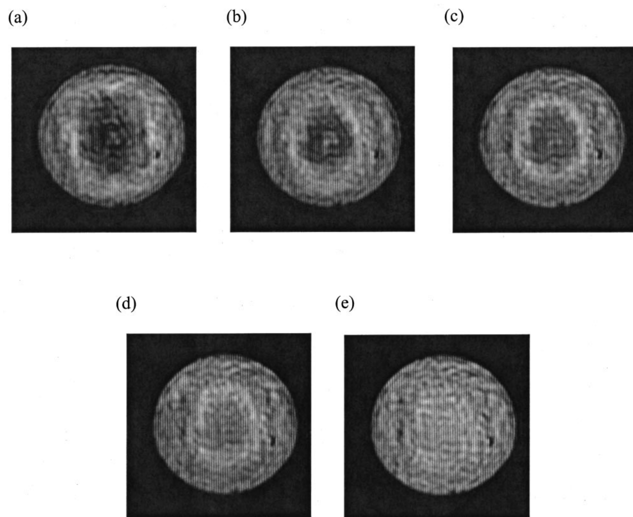

FIG. 4. (a)–(e) Holograms of 500, 300, 200, 100, and 70 nm opaque defects recorded on the CCD.

reconstruction of the image plane distribution. The almost perfect reconstructed Airy pattern is a result of the errors in the reference and object waves canceling each other out. In this configuration, the system essentially acts as a shearing interferometer, however, the object-side grating arrangement results in the shear being virtually zero, hence the sensitivity to aberrations is also nearly zero. This fortuitous result means that aberrations in the imaging optic will not adversely affect the imaging performance of the holographic defect reconstruction.

Figure 3(c) shows the defect-free intensity reconstruction after Fresnel propagation to the mask plane. This image effectively represents the illumination pattern at the mask plane and can be used to normalize subsequent images obtained in the presence of actual defects.

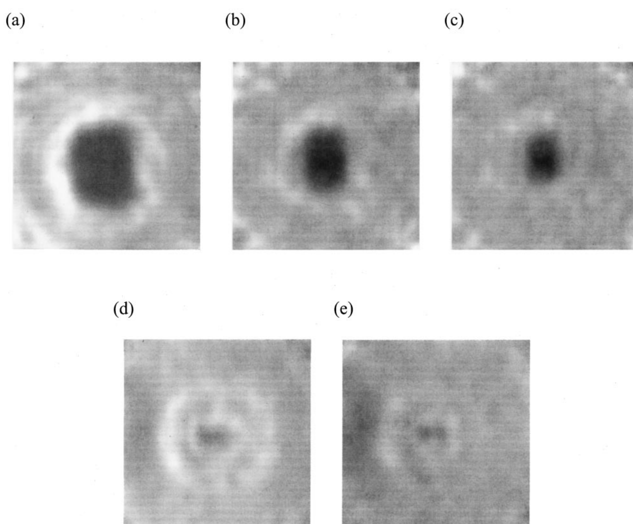

FIG. 5. (a)–(e) Reconstructed images of 500, 300, 200, 100, and 70 nm opaque defects, respectively. The lateral dimension of the reconstructed images is 1.7×1.7 μm. Square shapes of 500, 300, and 200 nm defects are clearly visible. The edges of the reconstructed images are a little blurry due to the nonrobust defect material. 100 nm defect is successfully reconstructed, but the detail shape of the defect is hard to be identified due to the resolution limit of the holographic microscopy.

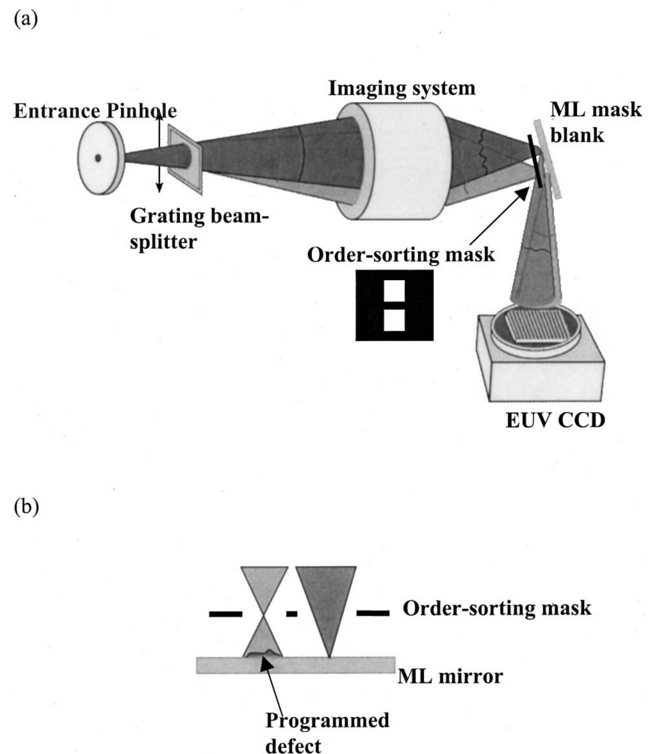

FIG. 6. (a) Proposed experimental schematic of a holographic microscope to characterize a reflective EUV multilayer mask blank. The same idea as with the transmission mask can be applied. The correct reflection angle is not shown. (b) Detailed view of the reflective mask region. The order-sorting mask is placed before the reflective mask. This mask would contain two free-standing windows respectively positioned on the two grating orders of interest.

Holograms for 500, 300, 200, 100, and 70 nm programmed opaque defects are shown in Fig. 4, and the corresponding reconstructed images of the defects are shown in Fig. 5. The reconstructed images cover an area of 1.7 μm $\times 1.7$ μm and have been normalized by the mask-plane illumination pattern [Fig. 3(c)], thereby, more accurately representing the transmittance of the mask. Square 500, 300, and 200 nm defects are clearly visible. The 100 nm defect is also successfully reconstructed, however, detailed shape information is lost due to the resolution limit of the holographic defect microscope. Observing the reconstruction of the 70 nm defect, we see that its shape is indistinguishable from that of 100 nm defect, however, the contrast is lower than the 100 nm defect case. We note that the rings around the small size defects are most likely artifacts from the normalization process and data analysis. The bandlimited coherent nature of the imaging process described here has the effect of producing ringing in the reconstructed images. Another source of ringing comes from the illumination itself which can be viewed as an out-of-focus coherent image of the Schwarzschild objective pupil. We have attempted to mitigate this second source of ringing through the normalization process

described above, however, uncorrelated speckle in the images renders this normalization incomplete.

The ultimate resolution of this system is set by the NA of the reference beam, which in turn is set by the NA of the image optic (0.088 in the case presented here). This NA corresponds to a resolution of approximately 100 nm. Characterization of smaller defects will require the use of a higher NA imaging system. However, as noted above, because aberrations in the imaging optic are effectively nulled out, it is not necessary to use an extremely high quality optic.

The characterization of phase defects on transmission masks is currently being studied. The experimental configuration would be identical to that described above with the exception of the programmed amplitude defects being replaced by programmed phase defects. The material to be used for the phase defects is Molybdenum which at a thickness of 86 nm provides a phase shift of π with only 40% attenuation.

IV. CHARACTERIZING REFLECTION MASKS

Here we have demonstrated the use of the holographic microscope for the characterization of opaque defects in transmission masks. To be a relevant tool for the development of EUV mask technology, however, the holographic microscope must be adapted to the characterization of reflection masks. A proposed configuration for such a device is depicted in Fig. 6.

The transmission mask used in the experiments described above is replaced by a EUV multilayer mask blank. The EUV mask is tilted allowing the reflected object and reference beams to be recorded on the CCD. The tilt angle should not exceed the multilayer angle bandwidth, which is typically less than 20°. The correct reflection angle is not shown in the picture (Fig. 6) in order to describe the system more easily. The implementation of this geometry may be more complicated by the limited angular bandpass of the multilayer masks.

To prevent extraneous orders from the grating beam splitter from corrupting the measurement, an order-sorting mask must be positioned between the imaging optic and the reflective test mask, Fig. 6(b). This mask would contain two freestanding windows, respectively, positioned on the two grating orders of interest. If the separation of the two windows is identical as the transmission mask case, the order sorting windows should be placed $\sim 12\ \mu$m from the multilayer mask surface.

In the proof-of-principle experiment described above, the mask was intentionally positioned out of focus allowing a larger area to be inspected. There was no concern of reference beam contamination because the reference window was kept clean (no defects on the reference window). In a practical situation, however, it is not possible to distinguish between the two beams. If both beams are of the same size on the sample, they will be equally likely to encounter defects and it will be hard to isolate individual defects. This potential problem can be minimized by making one of the two beams (the reference beam) significantly smaller on the sample. This could be achieved by adding optical power to the beam splitter grating allowing the zero and first-diffracted orders to be focused to different planes as shown in Fig. 6(b). The grating now effectively becomes a holographic optical element.

V. CONCLUSION

The use of holographic microscopy for the characterization of opaque defects in transmission masks has been successfully demonstrated at 13.4 nm wavelength. The biggest advantage of using a holographic technique is that both amplitude and phase information can be directly obtained. Amplitude defects of sizes ranging from 500 to 70 nm have been holographically reconstructed. The characterization of equivalently sized phase defects is currently under investigation. A proposed holographic microscope system to characterize defects on a reflective EUV multilayer mask blank has been introduced.

ACKNOWLEDGMENTS

This research has been supported by the Semiconductor Research Corporation under Contract No. 96-LC-460 and the DARPA Advanced Lithography Programs under Grant No. MDA972-97-0010. The authors would like to thank Erik Anderson for the transmission mask fabrications.

[1]D. Williamson, OSA Proc. EUV Lithography **23**, 68 (1995).
[2]S. Lee, P. Naulleau, K. A. Goldberg, and J. Bokor, Proc. SPIE **3997**, 823 (2000).
[3]S. Lee, P. Naulleau, K. Goldberg, C. Cho, and J. Bokor (unpublished).
[4]S. Burkhart, C. Cerjan, P. Kearney, P. Mirkarimi, C. Walton, and A. Ray-Chaudhuri, Proc. SPIE **3676**, 570 (1999).
[5]S. Jeong *et al.*, J. Vac. Sci. Technol. B **17**, 3009 (1999).
[6]J. Goodman, *Introduction to Fourier Optics,* 2nd ed. (McGraw-Hill, New York, 1996).
[7]K. A. Goldberg, P. Naulleau, and J. Bokor, J. Vac. Sci. Technol. B **17**, 2982 (1999).